High-Resolution Crosshole Radar Tomography: Application to Liquefaction-Induced Changes in Soil on Treasure Island

By Robert E. Kayen,[1] Walter A. Barnhardt,[1] Scott Ashford,[2] Kyle Rollins,[3] Diane L. Minasian,[1] and Bradley A. Carkin[1]

CONTENTS

Abstract

In 1998–99, the U.S. Geological Survey conducted a crosshole radar tomographic experiment at the lateral-pile-load testsite on Treasure Island to nondestructively image the soil column for changes in void ratio before and after a liquefaction event that was caused by controlled blasting. A geotechnical borehole radar technique was used to acquire high-resolution two-dimensional radar velocity data. This method of nondestructive site characterization uses transillumination surveys through the soil column and tomographic data-manipulation techniques to construct velocity tomograms, from which computed void ratios can be derived at 0.25- to 0.5-m-pixel footprints. Tomograms of void ratio are constructed by using a relation between soil void ratio and corresponding dielectric properties. The two-dimensional imagery is used to model changes in void ratio and to quantify void-ratio reduction in response to soil contraction during liquefaction. Predicted settlements based on planar-radar estimates of void-ratio reduction compare well with the observed settlements surveyed.

Introduction

This chapter describes a new nondestructive geophysical technique using ground-penetrating radar (GPR) to determine changes in soil void ratio due to the effects of liquefaction events. The void-ratio state of soil is principally controlled by depositional history, sedimentary texture, postdepositional load history, ground-water influence, and diagenetic changes to the soil fabric (Mitchell, 1993). Even subtle variations in environmental state and intrinsic physical properties can significantly alter the soil void ratio. The inplace void ratio of sand is typically estimated indirectly through empirical correlations with standard-penetration-test (SPT) and conventional cone-penetration-test (CPT) results. If a large budget is available, the inplace void ratio can be determined from laboratory analysis of frozen samples, or from neutron or gamma-ray density logging. The void-ratio state and sedimentary texture have a first-order influence on the liquefaction susceptibility of soils, and other factors (for example, particle orientation) are known to have a secondary influence (Seed and Idriss, 1982). This application of field crosshole GPR methods to characterize a potentially liquefiable soil mass is new, although early work on the relation between soil porosity and radar-band velocity dates back to Topp and others' (1980) the laboratory study using time-domain reflectometry (TDR).

Treasure Island is a hydraulically filled manmade structure in central San Francisco Bay, north of Yerba Buena Island, that was constructed for the 1939 Golden Gate International Exposition (fig. 1). The island was built in 1936 and 1937 by hydraulically pumping estuarine soil behind a perimeter rip-rap dike (fig. 1). Treasure Island is a National Geotechnical Experimentation Site (NGES), for which a considerable data set of geotechnical information is available. The soil profile at the testsite consists of hydraulically placed fill to 7-m depth, underlain by Holocene bay mud and older Pleistocene estuarine and terrestrial deposits. The hydraulic fill is primarily loose silty fine sand and sandy silt (Bennett, 1994). The water table is 1.0 to 1.5 m below the ground surface and was found to be fresh when we occupied the testsite.

The GPR-based technique for measuring soil-void-ratio changes complements a series of 10 full-scale pile-group and cast-in-steel-shell pile-load tests performed between December 1998 and February 1999 by researchers from the University of California, San Diego, and Brigham Young University, supported by the California Department of Transportation (Caltrans) and the National Science Foundation (Kayen and others, 2000). Other field data obtained from the testsite

[1]U.S. Geological Survey.
[2]University of California, San Diego.
[3]Brigham Young University.

included soil borehole logs, conventional CPT logs, and shear-wave-velocity profiles. All the testing at Treasure Island was conducted in cooperation with the U.S. Navy and the city of San Francisco (fig. 1).

The purpose of this study was to observe the effects of liquefaction on soil void ratio without the overprinting effect of mechanical lateral loading of the pile groups. To achieve this result, an array of three polyvinyl chloride (PVC)-cased

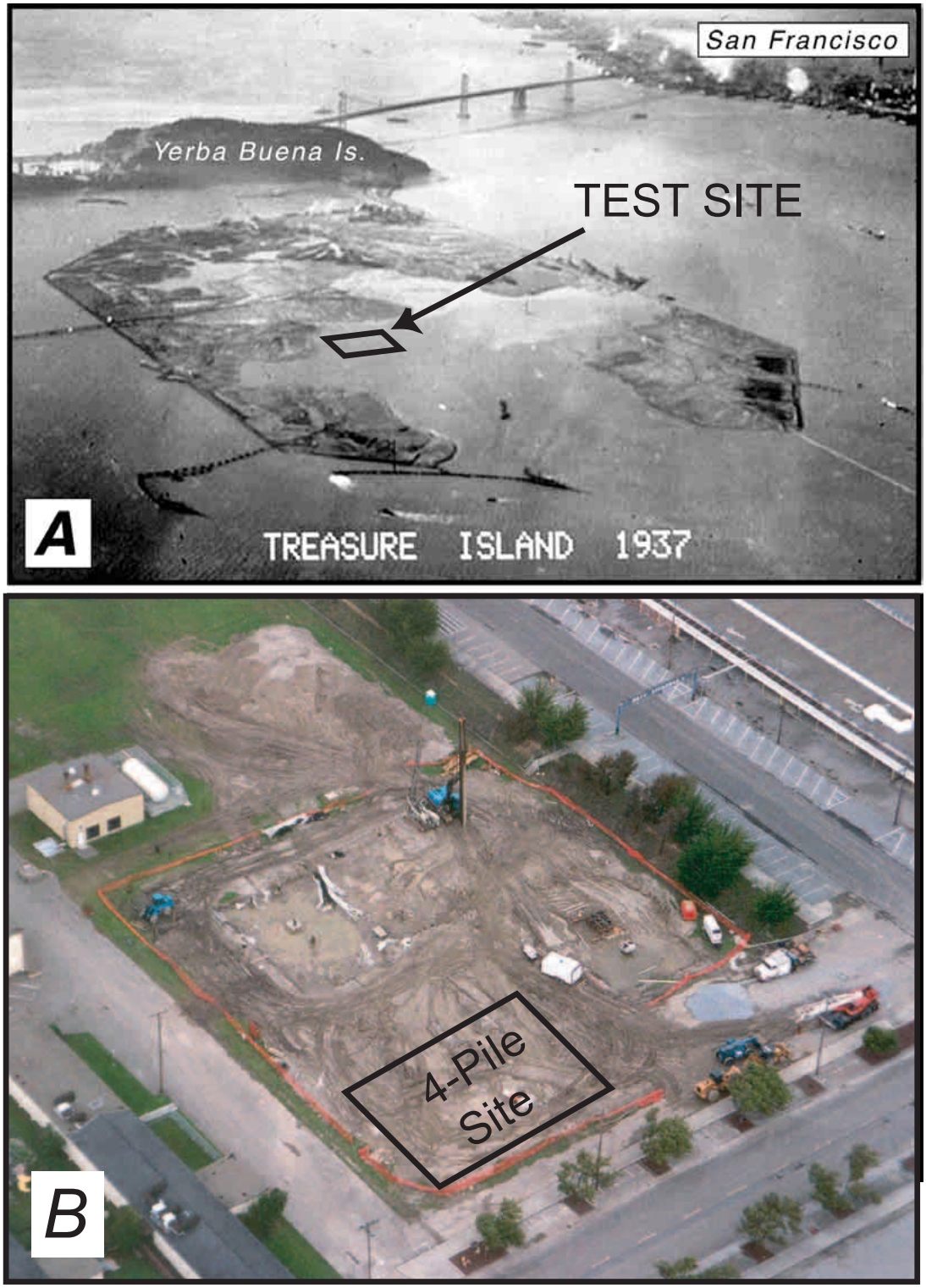

Figure 1.—Treasure Island in San Francisco Bay. *A*, Hydraulic filling in 1937. *B*, Radar and lateral-pile-load testsite (box) at intersection of Ninth and H streets near center of island.

boreholes were placed approximately 8 m away from the pile groups on the opposite side, equidistant from the blast charges. As such, the radar testsite was subjected to the same blast intensity as the pile group but isolated from pile-group loading after the blast. A drill rig augered each of the boreholes to 9-m depth and laid out the three boreholes in a 3–4–5-m triangular pattern. The holes were then cased with PVC liner.

Blasting

Blasts consisted of multiple sets of eight 0.5-kg explosive charges placed in circular patterns around the pile group. Each charge pattern had a diameter of approximately 5 m from the closest pile location and was approximately 5 m inside the radar borehole. The blasting was done in accord with the guidelines recommended by Studer and Kok (1980) and Narin van Court and Mitchell (1995). Paired charges were placed approximately 3.5 m below the excavated surface (approx 3 m below the ground-water table) and set off sequentially, with a short delay (250–1,000 ms) between charges to maximize the effect of the total blast on the soil mass. For each blast, pore-pressure time histories were collected, using horizontal and vertical pressure-transducer arrays, and peak particle velocity and settlements were measured.

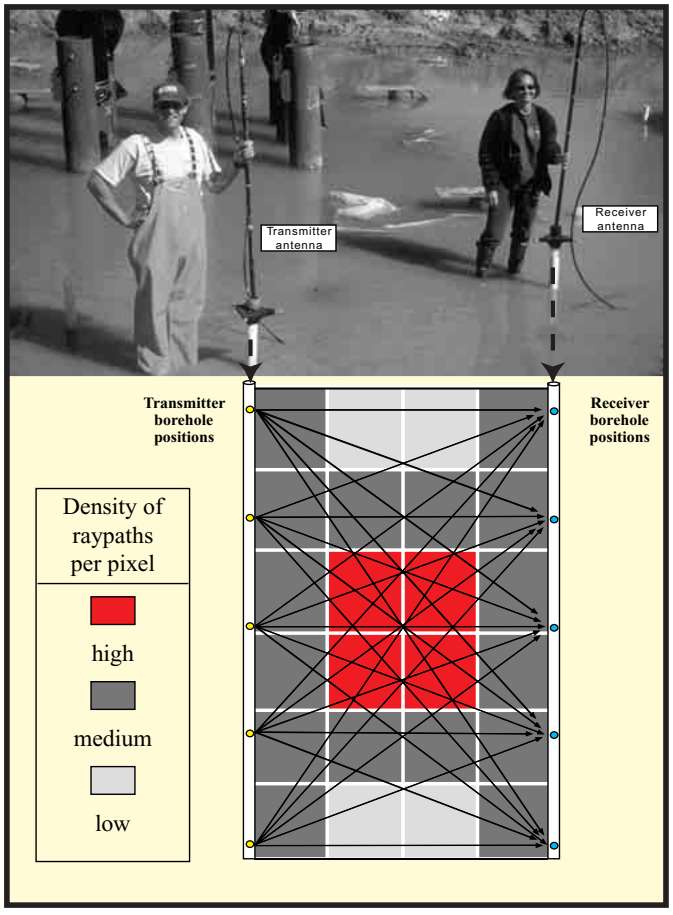

Figure 2.—Borehole radar investigation at Treasure Island testsite. Blast charges were placed between pile group and radar boreholes. Diagram shows below-ground raypaths shot and highest data density within central part of tomogram.

Radar Methods

Crosshole GPR is a transillumination survey method in which two antennas are lowered down adjacent, parallel boreholes. An example of how the antennas are deployed in the field is shown in figure 2. The transmitter antenna emits a short pulse, or shot, of high-frequency (here, 100 MHz) electromagnetic energy. The receiving antenna, located in the adjacent borehole, captures the frequency-modulated signal and precisely measures the time required for the signal to travel through the ground, along the plane separating the two boreholes. Traveltimes are one way, and measurements are made with picosecond (10^{-12} s) precision. Transillumination involves passing a waveform through the soil to determine the traveltime and attenuation characteristics of the wave (fig. 2). As such, crosshole GPR requires careful calibration of the outgoing waveform and shot-time zero to establish the signal traveltime. In the field, with antennas in fixed positions, multiple wave-trace records are recorded and stacked. Stacking involves adding together the waves of the multiple shots (32 in our survey) at each point along a profile. Stacking improves data quality by reinforcing the wave signal and suppressing noise. Field wave-trace records are immediately available to the researcher to assess the quality of the survey and individual waveforms.

The accuracy of the traveltime measurement is critical for determining the radar velocity. To determine the electronic-signal delay inherent in all circuits, the antennas are held outside each borehole, and a wave is transmitted through the air. For example, the two antennas shown in figure 2 are being held above the PVC boreholes to shoot a radar wave through the air. The speed of light in air and the borehole separation are known, and so the required wave traveltime can be computed. The electronic-signal delay is calculated as the recorded traveltime through sediment, minus the known time for an electromagnetic wave required to cross the borehole separation in air.

Two different types of crosshole survey were conducted: a constant-offset profile (COP) and a multiple-offset gather (MOG). The COP was used to make a quick reconnaissance survey of the testsite in which both GPR antennas were lowered to equal depths within their respective boreholes for each shot (fig. 3*A*). The COP allows for rapid collection of radio-wave velocities along a horizontal path (assumed bedding) direction, with an equal path length between transmitter and receiver all the way down the soil profile. We used the COP to rapidly identify, in the field, anomalies in traveltime and signal strength that would indicate variations in soil properties. COP data were also used to distinguish the hydraulic fill from bay mud and to design a plan for more detailed GPR surveys in the fill.

The MOG is a more detailed crosshole survey in which the transmitter antenna is fixed at a certain depth in one borehole while the receiver is moved in regular steps down the other

(fig. 3*B*). After the receiver collects shots from top to bottom (one complete MOG), the transmitter is lowered a predetermined step-interval and fixed at that new position, and the receiver is again moved down the other borehole. The process is repeated until the transmitter reaches the bottom. In this study, we collected a suite of MOGs, each with a step interval of 0.25 m. Unlike in a COP, the path length in an MOG varies widely from shot to shot. For each transmitter-receiver orientation, the path length is computed. In a perfectly homogeneous and isotropic medium, the first arrivals would form a hyperbola; deviations from a smooth hyperbolic pattern indicate variations in soil properties.

Tomographic Manipulation

Substantial computation, both in the field and in postacquisition processing, is required before interpretable images can be produced. After wave traces are gathered, the first and, if possible, second wave breaks must be picked. Refracted airwaves are common, especially when the antennas are near the surface, and must be distinguished from direct arrivals. This time-intensive process of event picking enables extraction of the traveltime, amplitude, and period of the transmitted pulse.

Tomographic analysis utilizes the path length and precise measurements of one-way traveltime to determine the velocity structure of the intervening materials. The positions of the transmitter and receiver antennas in the boreholes are well known, and so the raypath distance between the two antennas can be accurately calculated for each shot. The objective of conducting multiple surveys (COP and MOG) between the same boreholes is to collect traveltime data along as many raypaths and as many different angles as possible. The analysis first divides the single plane connecting the boreholes into a grid of cells, or pixels, and calculates the number of raypaths that intersect each cell. The result is a matrix of simultaneous velocity equations with a nonunique solution. The analysis then diverges from an initial estimated model of velocity structure (that is, horizontal layering) to find a "best fit" velocity with the observed data, performing multiple iterations and adjusting the model. The more raypaths or "hits" for each cell (pixel), the better the definition of transmission properties; fewer raypaths provide a less certain solution. Thus, data quality is commonly low at the corners and edges of tomographic images, and so we use only the high-quality data from the center (fig. 2*B*). For processing, all the COP and MOG traces were merged together into a single data set; first arrivals were picked, and a tomographic image was produced that shows the variations in veloc-

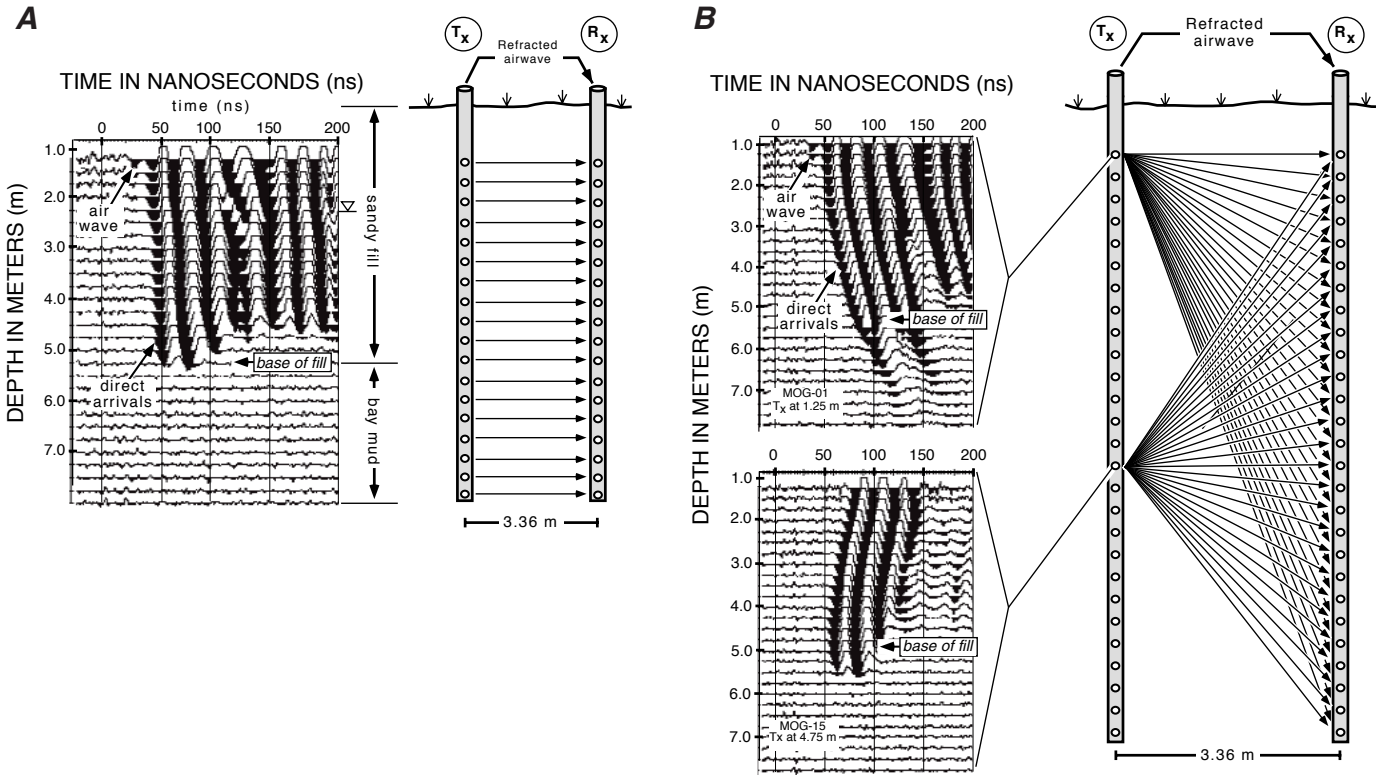

Figure 3.—Crosshole ground-penetrating-radar data and raypath configuration for constant-offset profile (*A*) and multiple-offset gather (*B*) on Treasure Island. Depths are relative to original ground surface. Tx, transmitter; Rx, receiver. Circles in boreholes, individual antenna positions. In figure 2*A*, absence of data below 5.25-m depth is due to signal attenuation by conductive bay mud that underlies sandy fill. Inverted triangle, approximate level of water table. In figure 2*B*, transmitter was fixed at a given position for each of 27 data files, only 2 of which are shown here. Depth scale indicates receiver position as it was lowered down borehole.

ity (fig. 4). Each transmitter-receiver path length was used to convert traveltimes to velocities within the illuminated plane. The pixel footprint within the resulting tomogram contains the velocity averaged from all the waveforms passing through each pixel space.

Relation of Void Ratio to Radar-Wave Velocity and Soil Dielectric Properties

The velocity of radar waves in the soil mass and in relation to saturated void ratio was studied empirically using the laboratory TDR method of Topp and others (1980). The traveltime of an electromagnetic pulse through a soil mass can be measured through reflection (two-way traveltime), refraction (headwave traveltime along an impedance interface), or transillumination (body transmission) techniques. At Treasure Island, we used a transillumination approach with crosshole GPR to measure traveltimes through a plane in the soil column. Two identical GPR surveys were collected, using the same pair of boreholes, one survey before blasting and another after blasting. A computer-generated tomogram was computed for each survey, showing the velocity structure of the same soil column both before (fig. 4*A*) and after (fig. 4*B*) the blast-induced liquefaction. MOGs were taken through the soil plane before and after blast-induced liquefaction, and a computer-generated tomogram was created for the plane.

The earliest study of the empirical relation between soil moisture content (equivalent to porosity when saturated) and radar velocity was by Topp and others (1980). With laboratory TDR, a method similar to our field approach with crosshole GPR, Topp and others determined a unique relation between volumetric soil moisture θ_v (ratio of volume of water to volume of total soil mass) and the real part of the complex dielectric constant for a wide variety of soil types. The complex dielectric constant of soil,

$$\varepsilon = \varepsilon' + \varepsilon'' j, \tag{1}$$

is composed of real (ε') and imaginary ($\varepsilon'' j$) parts. The radar velocity, v_r, depends only on

$$v_r = \frac{c}{\sqrt{\varepsilon'}}, \tag{2}$$

where c is the velocity of light in air. The ε' value ranges from 1 in air ($v_r = c = 0.3$ m/ns) to more than 30 in fine soil ($v_r \sim c/6 \sim 0.05$ m/ns). The v_r value ranges from less than 0.05 m/ns for soft cohesive soil, through 0.06–0.08 m/ns in saturated sand, to 0.15 m/ns in dry sand. For a suite of soil types, Topp and others (1980) determined the following relation between ε' and ε_v:

$$\varepsilon' = 3.03 + 9.3\theta_v^2 + 146\theta_v^2 - 76.7\theta_v^3 \quad (\theta_v = 0.0 - 0.6) \tag{3}$$

Saturated soils have all of their void space filled with water. Under such conditions, $\theta = n$, the soil porosity. Solving equation 3 for θ_v and assuming full saturation, n can be determined from ε' as follows:

$$n = -0.080607 + 0.037649\varepsilon' - 0.0011413(\varepsilon')^2 - 1.5789\times10^{-5}(\varepsilon')^3. \tag{4}$$

In the field, we measure radar velocity rather than dielectric constant. To estimate the soil porosity directly from radar velocity, we use the relation $\varepsilon' = (c/v_r)^2$ (where $c = 0.3$ m/ns) to modify equation 4, as follows:

$$n = 2.5025 - 75.54v_r + 920.1v_r^2 - 4{,}094.8v_r^3 \tag{5}$$

where v_r is in meters per nanosecond. The geotechnical characterization of a soil's density state is typically done in terms of void ratio (e), which is the void volume normalized by the volume of dry sediment grains. We substitute void ratio for porosity, where $e = n/(n-1)$, in equation 1 and solve for e in terms of ε' and v_r:

$$e = -0.035129 + 0.030695\varepsilon' - 3.553110^{-4}(\varepsilon')^2 + 9.6159\times10^{-6}(\varepsilon')^3 \tag{6}$$

and

$$e = 13.482 - 533.47v_r + 7{,}526.4v_r^2 - 36{,}615v_r^3. \tag{7}$$

Results: Void-Ratio Change During Liquefaction

We use equation 7 and the radar velocity determinations to map the soil void ratio before and after blast-induced soil liquefaction. The radar-velocity and void-ratio tomograms shown here (figs. 4–6) are from the 5-m-wide plane in the 3–4–5-m borehole triangle. To estimate void-ratio changes in the hydraulic fill, the degraded waveforms passing through the bay mud (fig. 4) were truncated from the data set so that an initial homogeneous velocity model could be used; including the bay mud in the data set added poorly constrained velocities. Void ratios before and after liquefaction were analyzed in the central part of the tomogram, on a plane extending from 2 to 4 m in depth and 0.75 to 2.6 m in width.

Before liquefaction, the plane was illuminated by GPR, and a velocity tomogram was constructed (fig. 4*A*). Equation 7 was used to convert the image to a preliquefaction void-ratio tomogram. The v_r value in the central part of the soil column at Treasure Island ranged from 0.054 to 0.6 m/ns, with an average of 0.057 m/ns. These v_r values translate into void ratios ranging from 0.647 to 0.846, with an average of 0.738 (fig. 5*A*). Generally, a zone of low to intermediate soil void ratio is present in the central part of the tomogram, and a zone of low soil void ratios in the upper-left part. A locally high soil void ratio is visible on the right side of the plane at 2.5- to 2.75-m depth, and a zone of higher void ratios in the lower-left corner of the tomogram.

The blasting event occurred in January 1999, liquefying the hydraulic fill at the testsite. Elevated pore-water pressures were measured in transducer arrays, sand boils were observed at the testsite, and settlements were surveyed and recorded.

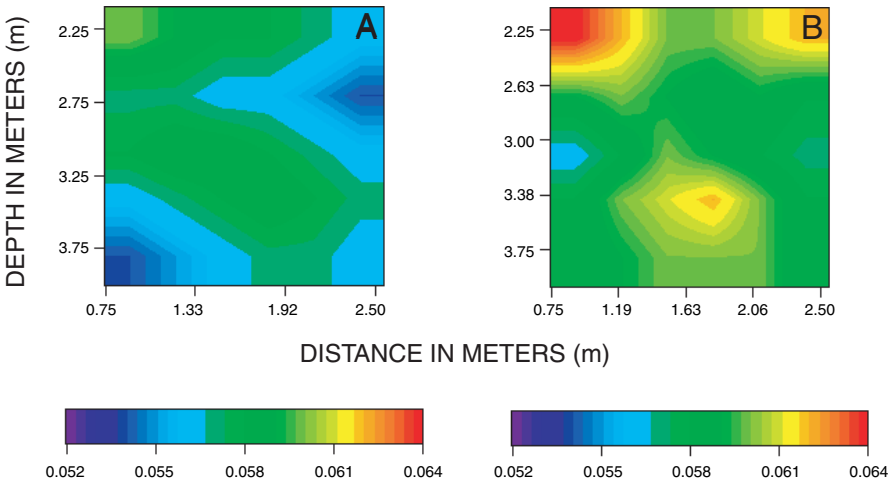

Figure 4.—Radar velocity across tomographic plane before (*A*) and after (*B*) blast-induced liquefaction event.

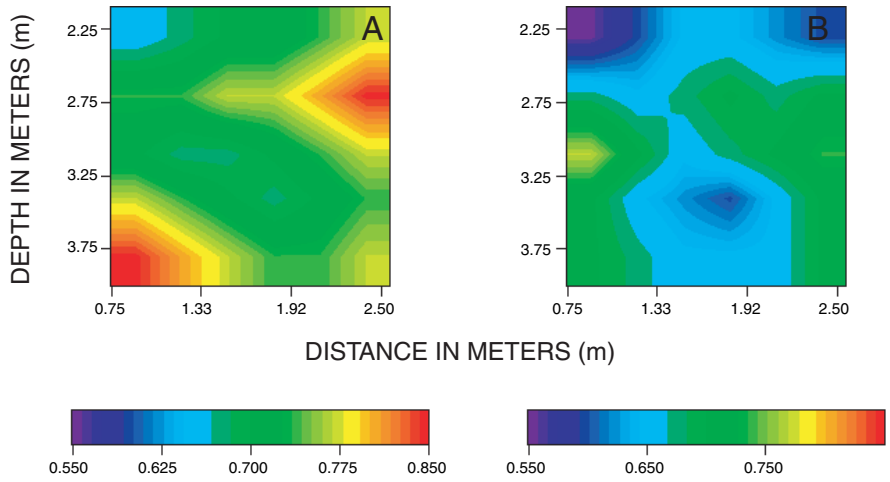

Figure 5.—Void ratio across tomographic plane before (*A*) and after (*B*) blast-induced liquefaction event.

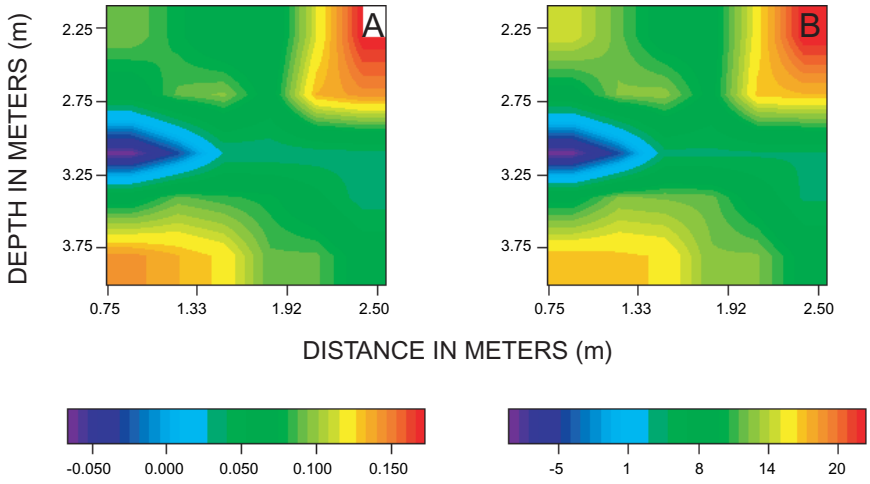

Figure 6.—Void-ratio change (*A*) and percent reduction (*B*) across tomographic plane after blast-induced liquefaction event.

Sand boils and waterflow to the surface was observed adjacent to the radar borehole array. Accordingly, we are confident that liquefaction occurred within the tomographic plane.

After the liquefaction, we resurveyed the 3–4–5-m triangular borehole array and found that v_r values had risen considerably throughout the tomogram. The v_r value for the postliquefaction soil plane ranged from 0.056 to 0.064 m/ns, with an average of 0.0597 m/ns (fig. 4*B*). The soil void ratios estimated from the v_r values range from 0.554 to 0.770, with an average of 0.664 (fig. 5*B*). Comparing figures 5*A* and 5*B*, almost the entire tomographic plane underwent some level of densification (void-space reduction) during liquefaction.

Detailed imagery of the preliquefaction and postliquefaction soil void ratios allows differencing of the two tomograms so that we can see where-void ratio changes occurred within the soil column. A difference tomogram of the preliquefaction minus the postliquefaction void ratios is shown in figure 6*A*. The image shows an average densification e of 0.074. The void-ratio change ranges from –0.066 to 0.172—that is, the entire tomographic plane densified except for a narrow zone at 3.1-m depth on the left side of the tomogram that apparently loosened during the liquefaction event or formed a void when sand redistributed within the soil column. Void-ratio change, expressed as a percentage of the initial state of void-ratio structure in the soil column (that is, volumetric strain), is plotted in figure 6*B*. The void-ratio change is calculated by taking the values used in figure 6*A* and dividing them by the initial void ratio, and so the regions of void-ratio change in figures 6*A* and 6*B* look similar. The average volumetric strain in the entire tomographic plane due to void-ratio reduction is 4.2 percent. Given the estimated thickness of the liquefied layer at the testsite of 4 to 5 m, this strain would result in 17.0 to 21.3 cm of one-dimensional vertical settlement (fig. 7).

The observed surface settlement at the testsite can be used as an independent measure of the volumetric strain. The ground level of the testsite was measured before blasting and then afterward. Maximum settlements of 16.7 to 20.7 cm were measured by Brigham Young University engineers along three transects across the testsite (fig. 9). One transect passed through the centerline of the pile group and load shaft, whereas the other two transects were perpendicular to that centerline. The settlements estimated from the volumetric strain recorded in the radar tomograms agree closely with the observed settlement. Arulanandan and Sybico (1993) reported comparable volumetric strains in liquefied sand during controlled centrifuge modeling tests conducted at the University of California, Davis.

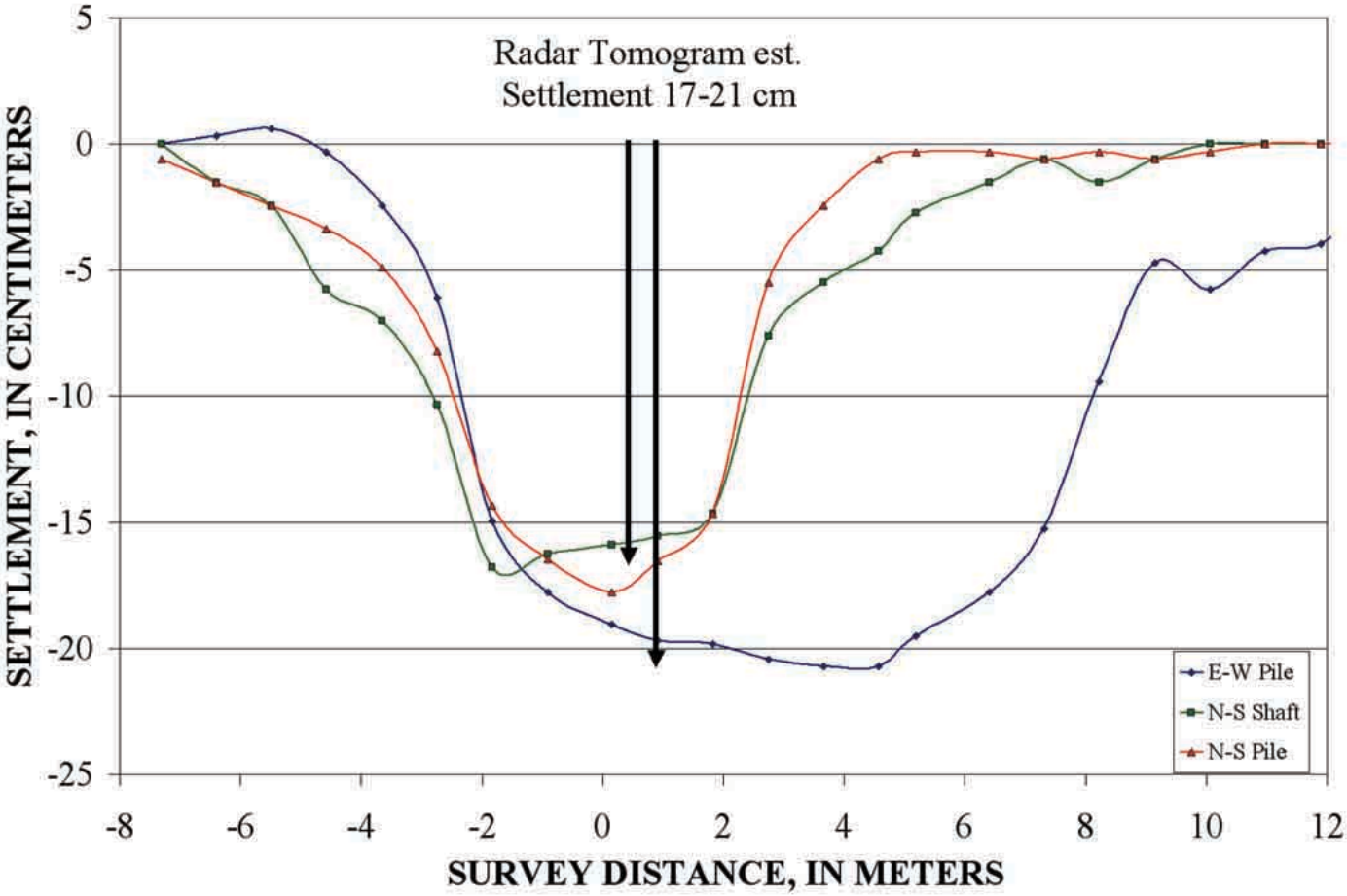

Figure 7.—Comparison of vertical settlements measured at lateral-pile-load testsite on Treasure Island and predicted settlements based on radar-velocity-determined volumetric strain for a 4- to 4.5-m-thick zone of liquefied soil.

Conclusions

We found that the imagery created through crosshole GPR surveys was able to quantify in spatial detail both the initial soil void ratio and the void-ratio changes due to a liquefaction event. The volumetric strain associated with the estimated void-ratio changes from the GPR data would result in settlements of 17 to 21.3 cm for the estimated 4- to 5-m-thick liquefied layer at the testsite. The radar-based estimates of settlement are remarkably close to the ground-level changes at the testsite measured by surveying methods.

This chapter demonstrates the applicability of crosshole GPR for nondestructive imaging of the spatial structure within a large volume of soil, as well as for characterization of the changes in soil volume due to a liquefaction event. The radar-based field observation of soil-fabric collapse and the quantified densification during liquefaction indicates that repeated loading should eventually drive the void ratio in the soil mass to the steady-state line.

References Cited

Arulanandan, Kandiah, and Sybico, J., Jr., 1993, Post-liquefaction settlement of sands, in Houlsby, G.T., and Schofield, A.N., eds., Predictive Soil Mechanics, Thomas Telford, London UK.

Bennett, M.J., 1994, Subsurface investigation for liquefaction analysis and piezometer calibration at Treasure Island Naval Station, California, U.S. Geological Survey Open-File Report 94–709, 43 p.

Kayen, R.E., Barnhardt, W.A., Ashford, S.A., and Rollins, Kyle, 2000, Nondestructive Measurement by crosshole radar tomography of soil density changes during liquefaction, Treasure Island, California, in Arulanandan, Kandiah, Anandarajah, Annaling-han, and Li, X.S., eds., Computer simulation of earthquake effects: American Society of Civil Engineers Geotechnical Publication 10, p. 52–65.

Mitchell, J.K., 1993, Fundamentals of soil behavior (2d ed.): New York, John Wiley & Sons, 437 p.

Narin van Court, W.A., and Mitchell, J.K., 1995, New insights into explosive compaction of loose, saturated, cohesionless soils, in Hyrciw, R.D., ed., Soil improvement for earthquake hazard mitigation: American Society of Civil Engineers Geotechnical Publication 49, p. 51–65.

Seed, H.B., and Idriss, I.M., 1982, Ground motions and soil liquefaction during earthquakes (Engineering Monographs on Earthquake Criteria, Structural Design, and Strong Motion Records, no. 5): Berkeley, Calif., Earthquake Engineering Research Institute, 134 p.

Studer, Jost, and Kok, Louk, 1980, Blast-induced excess porewater pressure and liquefaction; experience and application: International Symposium on Soils Under Cyclic and Transient Loading, Swansea, U.K., 1980, Proceedings, v. 1, pt. 2, p. 581–593.

Topp, G.C., Davis, J.L., and Annan, A.P., 1980, Electromagnetic determination of soil water content; measurement in coaxial transmission lines: Water Resources Research, v. 16, no. 3, p. 574–582.